J. Ocean Univ. China (Oceanic and Coastal Sea Research)
DOI 10.1007/s11802-014-1922-0
ISSN 1672-5182, 2014 13 (1): 45-50
http://www.ouc.edu.cn/xbywb/
E-mail:xbywb@ouc.edu.cn

Surface Heat Budget and Solar Radiation Allocation at a Melt Pond During Summer in the Central Arctic Ocean

ZHANG Shugang, ZHAO Jinping*, SHI Jiuxin, and JIAO Yutian

College of Physical and Environmental Oceanography, *Ocean University of China*, *Qingdao* 266100, *P. R. China*

(Received December 27, 2011; revised April 5, 2012; accepted December 20, 2012)

Abstract The heat budget of a melt pond surface and the solar radiation allocation at the melt pond are studied using the 2010 Chinese National Arctic Research Expedition data collected in the central Arctic. Temperature at a melt pond surface is proportional to the air temperature above it. However, the linear relationship between the two varies, depending on whether the air temperature is higher or lower than 0℃. The melt pond surface temperature is strongly influenced by the air temperature when the latter is lower than 0℃. Both net longwave radiation and turbulent heat flux can cause energy loss in a melt pond, but the loss by the latter is larger than that by the former. The turbulent heat flux is more than twice the net longwave radiation when the air temperature is lower than 0℃. More than 50% of the radiation energy entering the pond surface is absorbed by pond water. Very thin ice sheet on the pond surface (black ice) appears when the air temperature is lower than 0℃; on the other hand, only a small percentage (5.5%) of net longwave in the solar radiation is absorbed by such a thin ice sheet.

Key words heat budget; melt pond; solar radiation; Arctic

1 Introduction

Sea ice is one of the pivotal components of the global climate system, and changes in sea-ice extent, concentration, and thickness directly influence the absorbed solar radiation in the Arctic Ocean. Some general circulation model (GCM) results suggest that the Arctic sea ice not only influence the global climate but also is an indicator of global climate change (Rind *et al.*, 1995). The interaction between sea ice and solar radiation at the ocean surface is an important process that contributes to the reduction of sea-ice extent in the Arctic. A general trend of increasing solar heat input to the Arctic ice-and-ocean system is due to the decline in albedo induced by the decrease in ice concentration and by a longer melt season, and the largest increase occurred in the Chuchi Sea region, with a rate as large as 4% year^{-1} from 1979 to 2007 on average (Perovich *et al*., 2011). The Arctic Ocean receives the maximum solar radiation in mid August (Perovich, 2005). Sea ice melting is driven by shortwave radiation during the melting season (Light *et al*., 2008). While most of the solar radiation input to oceans happens over open waters, a substantial amount is also transmitted through sea ice and melt ponds. Hayes (2003) discovered that oceanic heat flux is influenced by shortwave radiation transmitted directly through ice. Perovich (2005) estimated that energy penetration through bare ice and pond-covered ice accounts for 23% and 16% of the shortwave radiation entering the ocean, respectively. For multi-year sea-ice packs, net longwave radiation and turbulent heat fluxes are the primary causes of heat loss, while shortwave radiation is the main cause of sea ice melting.

Melt ponds contribute significantly to the sea ice surface condition in summer, and occur extensively in the first-, the second-, and the multi-year ice. Melt ponds appear at the end of May, and occupy a significant portion of the sea ice surface by mid June. Ponds widen and deepen in June and July (sometimes melting through the ice layer), and begin to refreeze at the end of August or early September. By the beginning of October, they are indistinguishable from the rest of the ice pack (Fetterer and Untersteiner, 1998; Perovich *et al*., 2002). At the beginning of September, they have the maximum coverage, exceeding 50% of the sea ice surface (Flocco *et al*., 2010). Melt ponds influence energy and mass balances in various ways, such as altering the physical and optical properties of sea ice and refreezing at melt pond surfaces (Grenfell and Maykut, 1977; Perovich *et al*., 2002). The surface radiation and thermal properties of a melt pond differ distinctly from those of the surrounding sea ice. Studies have found that melt ponds play a key role in changing the albedo of sea ice. The albedo of bare ice and that of multi-year ice differ very little during the melting season; however, melt pond albedo varies greatly during the melting season (Perovich *et al*., 2002). And it decreases continually as the pond widens and deepens. Then

* Corresponding author. Tel: 0086-532-66782096
E-mail: jpzhao@ouc.edu.cn

the pond-covered ice absorbs a greater amount of solar radiation than bare ice, the melting rate beneath pond-covered ice is estimated to be up to 2–3 times greater than that of bare ice (Fetterer and Untersteiner, 1998).

The melt pond albedo is subject to rapid change, because the air temperature is frequently lower than 0℃ during the Arctic summer and melt pond surfaces are liable to refreezing. The fresh ice on the melt pond surface is less than 3-cm thick and usually lasts only a few days; thus, the magnitude of albedo of a refreezing pond is intermediate between open water and multi-year ice (Grenfell and Maykut, 1977). When sea ice melts, the brine is rejected from the ice and enters the pond to produce a very low salinity (Taylor and Feltham, 2004). The maximum density of melt pond water occurs when its temperature is approximately 3℃; when the melt pond temperature lies between 0℃ and 3℃ the lower the temperature is, the lower the density is (Taylor and Feltham, 2004). As a result of solar radiation, the density of the upper melt pond water is higher than that of the lower melt pond water, causing a vertical convective motion in the pond.

The occurrence of sea ice changes the heat exchange between the ocean and the atmosphere; similarly, the presence of melt ponds changes the heat budget of the sea ice surface. Furthermore, solar radiation is the main energy source for sea ice melting in summer in the central Arctic. Thus, it is important to quantitatively examine the heat budget of the melt pond surface and the solar radiation allocation at the melt pond.

2 Measurements

Observations of melt pond depth and radiation properties were carried out at a long-term ice station (initial location: 86°30′N, 172°24′W) maintained by the Chinese National Arctic Research Expedition from July to September 2010. Upward and downward shortwave radiations (0.3–2.8 μm) and longwave radiations (4.5–42 μm) at one of the melt ponds were measured using a radiometer CNR4 (Kipp & Zonen Company), as is shown in Fig.1. The shape and surface condition of the melt pond were recorded by a camera. Air temperature was measured using a CNR4 at 10 min intervals. Wind speed, relative humidity, and total cloud cover were recorded at 00:00, 6:00, and 12:00 Universal Time (UT) each day.

Fig.1 Measurement of radiation at the melt pond surface with radiometer CNR4.

3 Results

Air temperature, wind speed, and relative humidity for the period August 12–18 are shown in Fig.2; they changed significantly around August 17. The air temperature (red line) was lower than 0℃ from August 12 to 16, the lowest of which was about −4.0℃ on August 15. From August 17, it rose above 0℃, the maximum being approximately 2℃. The wind speed (blue line) increased rapidly from 1 m s^{-1} on August 16 to 12 m s^{-1} on August 17. The relative humidity (black line) quickly decreased at the beginning of August 17. The entire melt pond surface was covered by newly formed ice on August 15, but it lasted only for less than a day. Black ice was observed on the melt pond surface only before August 17, with a thickness less than 1 cm during the observation period.

The downward solar radiation (F_{sd}), upward solar radiation (F_{su}), downward longwave radiation (F_{ld}), upward longwave radiation (F_{lu}), and net longwave radiation (N_l= F_{ld}−F_{lu}) are shown in Fig.3. They indicate that the F_{lu} (green line) and F_{ld} (red line) were stronger than F_{ld}

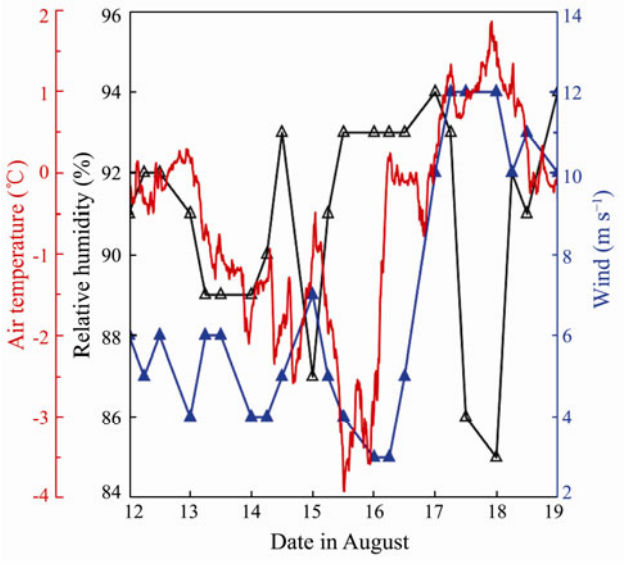

Fig.2 Time series of air temperature (red), relative humidity (black), and wind speed (blue).

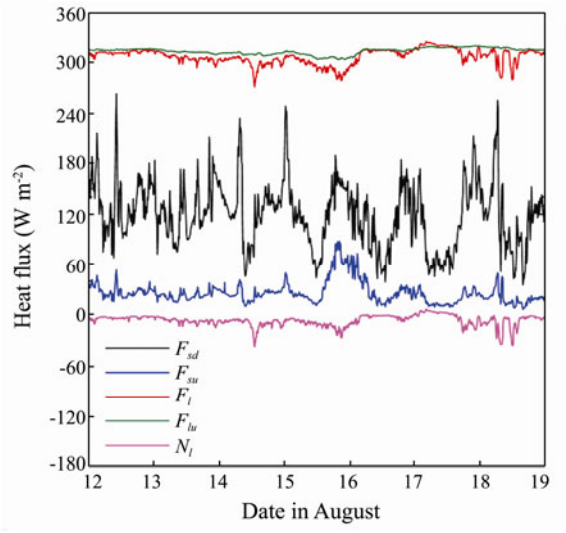

Fig.3 Time series of F_{sd} (black), F_{su} (blue), F_{ld} (red), F_{lu} (green), and N_l (magenta).

(black line), but the N_l was relatively weak and smaller than zero. Thus, the melt pond lost some energy in the form of N_l. Because the melt pond had a lower albedo and absorbed a large amount of solar energy, F_{su} was relatively small.

The observations suggest that air temperature, relative humidity, wind speed, and the melt pond surface changed around August 17. Was there an obvious change in the heat budget of the melt pond surface because the black ice disappeared?

3.1 Heat Flux Calculation for the Melt Pond Surface

The heat fluxes, including F_{sd}, F_{su}, F_{ld}, F_{lu}, F_{sp} (sensible-heat flux), and F_{ep} (latent-heat flux), are related to the state of the melt pond surface. Due to the influence of black ice, the heat flux through the melt pond surface varied from August 12 to August 18. Assuming the downward flux is positive (the ocean gains heat), the upward flux from the ocean surface into the atmosphere is then negative. The net heat flux (N_r) across the melt pond surface can be written as

$$N_r = F_{sd} - F_{su} + F_{ld} - F_{lu} + F_{sp} + F_{ep}\,, \tag{1}$$

where F_{sd}, F_{su}, F_{ld}, and F_{lu} can be measured directly using a radiometer CNR4. The turbulent heat fluxes (F_{sp} and F_{ep}) can be obtained as in Maykut (1978, 1982):

$$F_{sp} = \rho_a c_p C_s u(T_a - T_w) \tag{2}$$

and

$$F_{ep} = \frac{0.622\rho_a L_v C_e}{P_0} u(re_{sa} - e_{sw})\,, \tag{3}$$

where ρ_a=1.3 kg m^{-3} is the average air density, c_p=1005.0 J kg^{-1} K^{-1} is the specific heat of the air, L_v=2.49 MJ kg^{-1} is the latent heat of vaporization, P_0=1013 mbar is the surface pressure, C_s=1.75×10^{-3} is the transfer coefficient for sensible heat, C_e=C_s is the transfer coefficient for latent heat, T_a is the air temperature, T_w is the melt pond surface temperature, e_{sa} is the air saturation vapor pressure, e_{sw} is the melt pond surface saturation vapor pressure, u is the wind speed, and r is the relative humidity. When the temperature is higher than −20℃, the relationship between saturation vapor pressure and temperature can be written as (Maykut, 1978, 1982)

$$e_s = b_1T^4 + b_2T^3 + b_3T^2 + b_4T + b_5\,, \tag{4}$$

where

$$b_1 = 2.7798202\times10^{-6}\,,$$

$$b_2 = -2.6913395\times10^{-3}\,,$$

$$b_3 = 0.97920849\,,$$

$$b_4 = -158.63779\,,$$

$$b_5 = 9653.1925\,.$$

The air and melt pond surface saturation vapor pressures (e_{sa} and e_{sw}) can then be calculated using T_a and T_w according to Eq. (4). Then F_{sp} and F_{ep} can be calculated using Eqs. (2) and (3), respectively.

The air temperature, relative humidity, and wind speed can be directly measured; however, the melt pond surface temperature is difficult to measure because of the influence of black ice. According to the Stefan–Boltzmann law, T_w can be derived from F_{lu}, which is measured by a CNR4,

$$F_{lu} = \varepsilon\sigma T_w^4\,, \tag{5}$$

where σ (=5.67×10^{-8} J m^{-2} s^{-1} K^{-4}) is the Stefan-Boltzmann constant and ε is the longwave emissivity of the melt pond. A melt pond on top of the ice in summer is almost a black body at infrared wavelengths (Sandven and Johannesen, 2006), therefore ε is set equal to unity.

3.2 Heat Budget of the Melt Pond Surface

As seen from Fig.4, the time change of T_w (red line) corresponds to T_a (black line). When T_a is bellow 0℃, T_w is also lower than 0℃ but higher than T_a, for the black ice cover exists; while T_a was higher than 0℃, T_w was lower than T_a when free of black ice coverage. In addition, T_w responses to changes in the melt pond surface condition.

Fig.5 is a scatter plot of T_a and T_w, which demonstrates a good linear relationship that switches at T_a=0℃. When T_a is lower than 0℃, the correlation coefficient (r), root-mean-square (RMS) error, and the linear relationship between T_a and T_w are 0.988, 0.006, and $T_w^{'}$=0.69T_a−0.028, respectively. When T_a is higher than 0℃, the corresponding values are 0.973, 0.002, and $T_w^{'}$=0.56T_a−0.058, respectively. The above comparison suggests that the correlation coefficient and the slope when T_a is lower than 0℃ are larger than those when T_a is higher than 0℃. The main reason is that the surface conditions of the melt pond changed from August 12 to 18 (Fig.1).

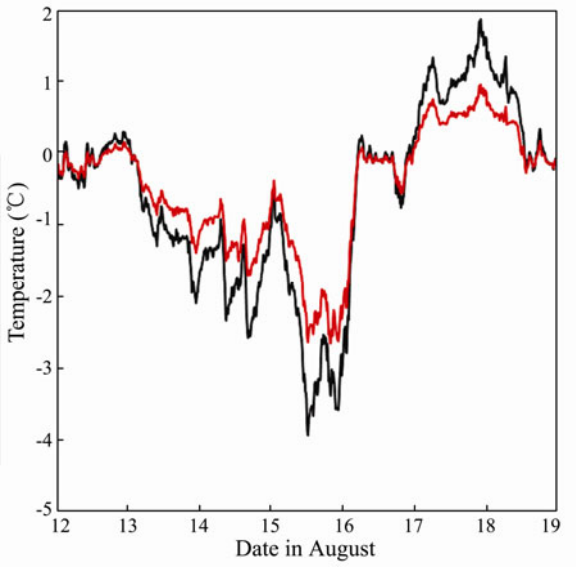

Fig.4 Time series of T_w (red) and T_a (black).

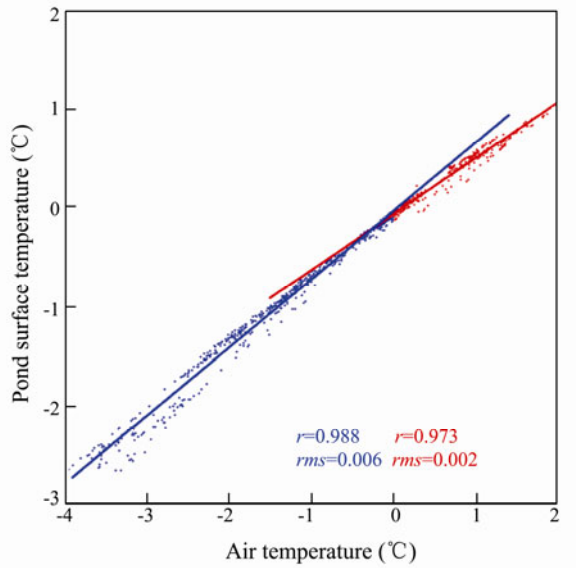

Fig.5 Scatter plot of T_a and T_w. The latter r represents correlation coefficient, and *rms* indicates root-mean-square error. Blue corresponds to the air temperature lower than 0℃, and red is for the air temperature higher than 0℃.

N_r, F_{sp}, and F_{ep} are calculated using Eqs. (1), (2), and (3) when T_w is obtained. They are shown in Fig.6, which include N_e and N_s=F_{sd}−F_{su}, the net shortwave radiation of the melt pond. We can see that N_r and N_s has a diurnal cycle; N_l, F_{sp}, and F_{ep} are relatively small compared with N_r; both N_l and F_{ep} are negative. F_{sp} is negative from August 12 to 16, but is positive after August 17 due to the change of T_a. The above discussion suggests that the melt pond heat loss is a combined effect of F_{sp}, F_{ep}, and N_l during August 12–17, and it gain some energy in the form of sensible heat after August 17.

Light *et al*. (2008) stated that sea ice usually loses heat in the form of longwave radiation and turbulent (sensible and latent) heat fluxes in multi-year ice regions. The total turbulent heat flux of the melt pond surface can be written as F_t=F_{ep}+F_{sp}. Two stages (August 12–16 and August 17–18) were considered in terms of heat fluxes at the melt pond surface because air temperature, wind speed, relative humidity, and melt pond surface conditions underwent obvious change on August 17. During the first stage, the air temperature was lower than 0℃, and black ice with thicknesses smaller than 1 cm was present on the melt pond surface. During the second stage, the air temperature was greater than 0℃, and black ice disappeared. The heat fluxes during the two stages are shown in Table 1. We can see that the melt pond surface always loses heat in the form of N_l and F_t, with the later being the main cause. In the first stage, F_t was more than twice the amount of N_l. Although F_t decreased because of F_{sp} in the second stage, it was higher than longwave radiation during the second stage. Thus, the melt pond lost most heat when the air temperature was lower than 0℃.

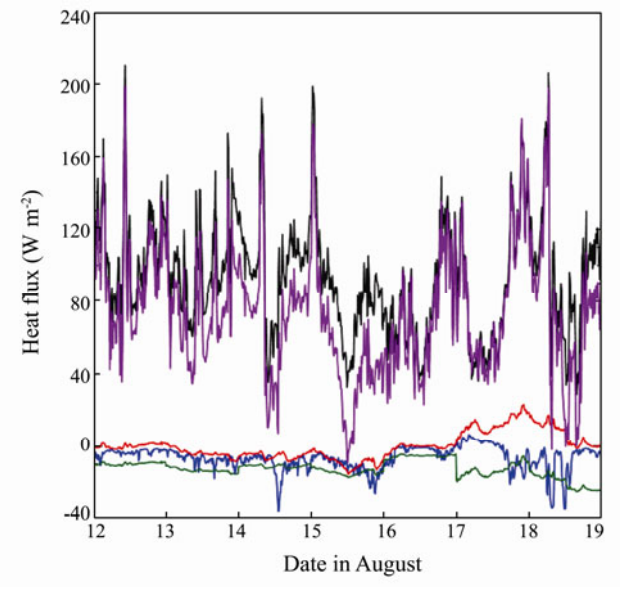

Fig.6 Time series of melt pond surface heat budget: N_r (purple), N_s (black), N_l (blue), F_{sp} (red), and F_{ep} (green).

Table 1 Heat budget of the melt pond surface

Date (mm/dd)	Heat budget (W m^{-2})			
	N_s	N_l	F_t	N_r
08/12–08/16	94.3	−6.9	−14.4	73.1
08/17–08/18	91.3	−6.0	−7.2	78.1
08/12–08/18	93.4	−6.6	−12.3	74.6

4 Solar Radiation Allocation at the Melt Pond

4.1 Solar Radiation Attenuation

Due to the lower albedo of the melt pond, a large amount of solar radiation is absorbed in the pond. The absorption of solar radiation (F_p) in the melt pond is parameterized by the following equation from Ebert and Curry (1993):

$$F_p = F_{sd}(a_p + a_p\alpha_i t_p), \quad (6)$$

where α_i=0.65 is the albedo of multi-year ice (Grenfell

and Perovich, 1984; Pegau and Paulson, 1999), t_p is the pond transmissivity, which is a function of melt pond depth (h_p) in the form t_p=0.36−0.17log$_{10}$(h_p) (Neumann and Pierson, 1966; Ebert and Curry, 1993), a_p is the absorption coefficient of the melt pond with $a_p = 1 - t_p^{0.89}$ (Neumann and Pierson, 1966; Ebert and Curry, 1993).

The amount of solar radiation transmitted through the pond and into the ice (F_i) is given by

$$F_i = F_{sd} - F_{su} - F_p \,. \tag{7}$$

The melt pond depth changed between 0.5 and 0.53 m during the observation period. The absorption of solar radiation changed very little according to the calculated results of Eq. (6). Thus, the melt pond depth is set to 0.52 m in the calculation.

Black ice of thickness lower than 1 cm floated at the melt pond surface from August 12 to 16. The absorbed of radiation penetrating the black ice can be calculated according to the Bouguer-Lambert law:

$$I_i = F_{ds}(1 - e^{-\kappa h}) \,, \tag{8}$$

where κ is the extinction coefficient of black ice, equal to 0.6–0.8 m^{-1} (Bolsenga, 1978; Heron and Woo, 1994), and h is the thickness of the black ice. The proportion of Fsd absorbed by black ice is lower than 0.8%, from Eq. (8) with κ equal to 0.8 m^{-1} and the black ice thickness equal to 0.01 m. The actual thickness of the black ice was less than 0.01 m, so the amount of radiation absorbed by the black ice can be ignored.

4.2 Downward Solar Radiation Allocation

The melt pond loses energy in the form of N_l and F_t, which are both derived from F_p. Thus, the net absorption of solar radiation N_p by the melt pond is calculated as

$$N_p = F_p - F_t - N_l \,. \tag{9}$$

The above analysis indicates that some solar radiation is reflected at the melt pond surface, some is transmitted through the pond and into the ice, and the rest is absorbed by the melt pond water. F_p releases some energy into the atmosphere in the form of N_l and F_t. The allocation of solar radiation at the melt pond surface and in its interior can be expressed by

$$F_{sp} = F_{su} + F_i + F_t + N_p + N_l + I_i \,. \tag{10}$$

The allocation of F_{sd} is shown in Figs.7a and 7b for August 12–6 and August 17–18, respectively. Some solar radiation was absorbed by the black ice from August 12 to 16 because of the occurrence of black ice. This fraction was around 0.8% when the thickness of the black ice was 0.01 m and the extinction coefficient was 0.8 m^{-1}. In actuality, the fraction would be lower than 0.8%. The reflected solar radiation, which indicates the albedo of the melt pond, is obviously influenced by the black ice. The mean reflected fraction was 23.2% during August 12–16; however, it decreased to 17.3% during August 17–18. Fig.6 indicates that F_{sp} was positive after August 16, and F_{ep} was always negative. Thus, under the influence of F_{sp}, the mean fraction of the turbulent heat flux was only 6.5% during August 17–18, but was nearly doubled (11.6%) during August 12–16. The mean fraction of N_l changed very little during the study period (around 5.5%). During August 12–16, 51.8% of the solar radiation was absorbed by the melt pond and 7.1% of it entered the sea ice; however, during August 17–18, 57.7% and 13.1% of the solar radiation were absorbed by the melt pond and the sea ice, respectively. Because of the influence of black ice and air temperature, the allocation of solar radiation at the melt pond surface and the interior was altered. Fig.7 suggests that a large amount of solar radiation (exceeding 50%) was absorbed by the melt pond, which would cause sea ice to melt and pond water temperature to increase.

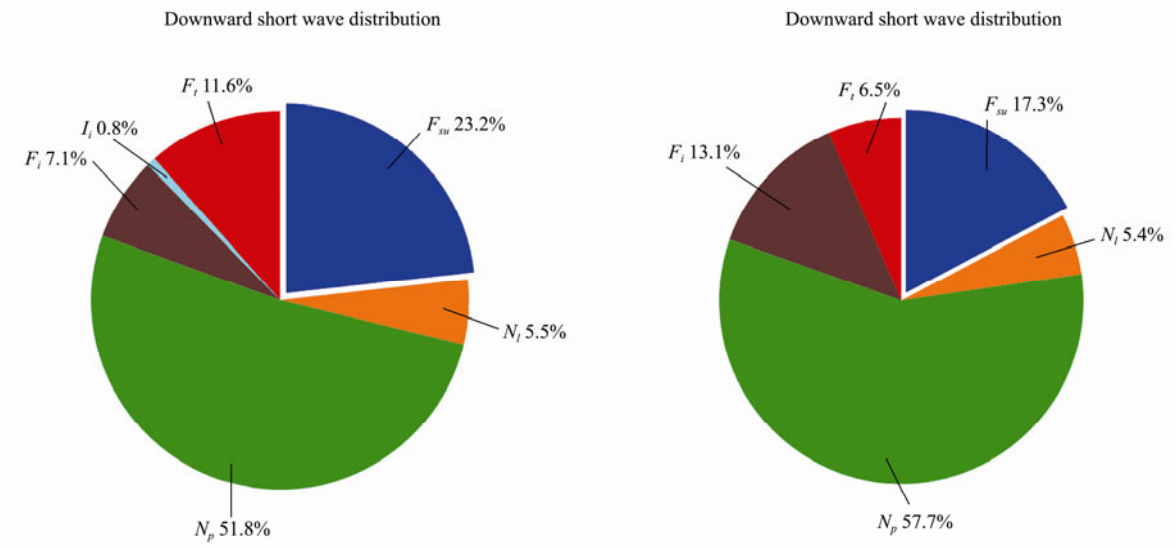

Fig.7 Allocation of solar radiation at the melt pond surface and its interior. (a) mean during August 12–16; (b) mean during August 17–18.

5 Conclusions

In the central Arctic, an increasing proportion (may exceed 50%) of melt pond exists on sea ice, which alters the thermal budget and energy balance. It is very important to reveal the properties of melt pond using *in situ* measurements, with which the solar radiation allocation in the melt pond can be neatly estimated. In this study, the heat budget of the a melt pond is quantitatively examined.

1) The melt pond surface temperature is proportional to the air temperature, but the linear relationship between the two changes when the air temperature reaches 0℃. The correlation coefficient and the linear relationship are 0.988 and $T_w^{'} = 0.69T_a - 0.028$ when the air temperature is lower than 0℃. However, they are 0.973 and $T_w^{'} = 0.56T_a - 0.058$ when the air temperature is greater than 0℃. Thus, when the air temperature is lower than 0℃, the melt pond surface temperature is relatively more remarkably affected by air temperature.

2) The melt pond loses energy in the form of net longwave radiation and turbulent heat fluxes, with the latter contributing more to the surface thermal budget. When the air temperature is lower than 0℃, the surface heat flux is outward and the total turbulent heat flux is more than twice the energy by net longwave radiation. When the air temperature is higher than 0℃, the melt pond receives some energy through sensible-heat flux, but the total turbulent heat flux is outward because of stronger latent-heat flux.

3) The allocation of solar energy in the pond is estimated by the directly measured data at an ice camp. More than 50% of the radiation energy incident on the pond surface is absorbed by the pond water. Very thin (about 1 cm) black ice on the pond surface appeares under cold conditions, but the measured results suggest that the solar energy absorbed by such a thin ice sheet can be neglected.

Acknowledgements

This study is supported by the Global Change Research Program (2010CB951403), the Major National Science Research Program (2013CBA01805) and the Open Research Fund of the State Oceanic Administration of the People's Republic of China Key Laboratory for Polar Science (3KP201203). We thank the expedition members and the *R/V Xuelong* crew for their help.

References

Bolsenga, S. J., 1978. *Photosynthetically Active Radiation Transmittance Through Ice*. Great Lakes Environmental Research Laboratory & Environmental Research Laboratories, NOAA Technical Memorandum, ERL GLERL-18, 48pp.

Ebert, E. E., and Curry, J. A., 1993. An intermediate one-dimensional thermodynamic sea ice model for investigating ice-atmosphere interactions. *Journal of Geophysical Research*, **98** (C6): 10085-10109.

Fetterer, F., and Untersteiner, N., 1998. Observations of melt ponds on Arctic sea ice. *Journal of Geophysical Research*, **103** (C11): 24821-24835.

Flocco, D., Feltham, D. L., and Turner, A. K., 2010. Incorporation of a physically based melt pond scheme into the sea ice component of a climate model. *Journal of Geophysical Research*, **115** (C08012), DOI: 10.1029/2009JC005568.

Grenfell, T. C., and Maykut, G. A., 1977. The optical properties of ice and snow in the Arctic Basin. *Journal of Glaciology*, **18**: 445-463.

Grenfell, T. C., and Perovich, D. K., 1984. Spectral albedos of sea ice and incident solar irradiance in the Southern Beaufort Sea. *Journal of Geophysical Research*, **89**: 3573-3580.

Hayes, D. R., 2003. *The Heat and Salt Balances of the Upper Ocean Beneath a Spatially Variable Melting Sea Ice Cover*. University of Washington, 296pp.

Heron, R., and Woo, M. K, 1994. Decay of a high Arctic lake-ice cover: Observations and modeling. *Journal of Glaciology*, **40**: 283-292.

Light, B., Grenfell, T. C., and Perovich, D. K., 2008. Transmission and absorption of solar radiation by Arctic sea ice during the melt season, *Journal of Geophysical Research*, **113**, C03023, DOI: 10.1029/2006JC003977.

Maykut, G. A., 1978. Energy exchange over young sea ice in the central Arctic. *Journal of Geophysical Research*, **83**: 3646-3658.

Maykut, G. A., 1982. Large-scale heat exchange and ice production in the central Arctic. *Journal of Geophysical Research*, **87**: 7971-7984.

Neumann, G., and Pierson, W. J., 1966. *Principles of Physical Oceanography*. Prentice-Hall, Englewood Cliffs, NJ, 545pp.

Pegau, W. S., and Paulson, C. A., 1999. The effect of clouds on the albedo of Arctic leads. *Eos Trans. AGU*, Abstract F221, **80**: 46.

Perovich, D. K., Grenfell, T. C., Light, B., and Hobbs, P. V., 2002. Seasonal evolution of the albedo of multiyear Arctic sea ice. *Journal of Geophysical Research*, **107** (C10), 8044, DOI: 10.1029/2000JC00438.

Perovich, D. K., 2005. On the aggregate-scale partitioning of solar radiation in Arctic sea ice during the Surface Heat Budget of the Arctic Ocean (SHEBA) field experiment. *Journal of Geophysical Research*, **110**, C03002, DOI: 10.1029/2004JC002512.

Perovich, D. K., Jones, K. F., Light, B., Eicken, H., Markus, T., Stroeve, J., and Lindsay, R., 2011. Solar partitioning in a changing Arctic sea-ice cover. *Annals of Glaciology*, **52** (57): 192-196.

Rind, D., Healy, R., Parkinson, C., and Martinson, D., 1995. The role of sea ice in $2\times CO_2$ climate model sensitivity, Part I, the total influence of sea ice thickness and extent. *Journal of Climate*, **8**: 449-463.

Sandven, S., and Johannessen, O. M., 2006. *Sea Ice Monitoring by Remote Sensing*. The American Society for Photogrammetry & Remote Sensing, Chapter 8, 13pp.

Taylor, P. D., and Feltham, D. L., 2004. A model of melt pond evolution on sea ice. *Journal of Geophysical Research*, **109**, C12007, DOI: 10.1029/2004JC002361.

(Edited by Xie Jun)